Effect of Pressure on a Multicomponent A/B/A−C Polymer Blend with Attractive and Repulsive Interactions

Megan L. Ruegg,[†] Benedict J. Reynolds,[†,‡] Min Y. Lin,[||,#] David J. Lohse,[||] Ramanan Krishnamoorti,[⊥] and Nitash P. Balsara*[,†,§]

Department of Chemical Engineering, University of California, Berkeley, California 94720; Earth Science Division, Lawrence Berkeley National Laboratory, University of California, Berkeley, California 94720; Materials Sciences Division and Environmental Energy Technologies Division, Lawrence Berkeley National Laboratory, University of California, Berkeley, California 94720; ExxonMobil Research and Engineering, Annandale, New Jersey 08801; and Department of Chemical Engineering, University of Houston, Houston, Texas 77204

Received August 16, 2006; Revised Manuscript Received September 28, 2006

ABSTRACT: The effect of pressure on the phase behavior of a multicomponent polymer blend was studied by small-angle neutron scattering (SANS). The blend was composed of saturated polybutadiene with 89% 1,2-addition (component A), polyisobutylene (component B), and an A−C diblock copolymer, where block A was chemically identical to component A and block C was a saturated polybutadiene with 63% 1,2-addition (sPB63). At atmospheric pressure, the blend forms a lamellar phase at low temperature, forms a microemulsion phase at intermediate temperatures and is macrophase separated at high temperatures. No evidence of homogeneous phases was found at atmospheric pressure. Upon pressurization the A/B/A−C blend exhibited a homogeneous phase across a wide range of pressures and temperatures. The pressure dependencies of the Flory−Huggins interaction parameters in this system (χ_{AB}, χ_{AC}, χ_{BC}) were determined from SANS measurements on binary blends and used to model the thermodynamic properties of the multicomponent blend as a function of temperature and pressure with the random phase approximation, self-consistent-field theory, and Flory−Huggins theory. We demonstrate excellent agreement between theory and experiment without any adjustable parameters.

Introduction

The fact that the thermodynamic properties of polymer mixtures are affected by temperature and pressure is well established. In the case of simple systems such as mixtures of polyolefins, Flory−Huggins theory[1,2] provides a framework for understanding these effects in terms of intermolecular interactions.[3] Most binary homopolymer mixtures phase separate upon cooling; i.e., they exhibit an upper critical solution temperature or UCST behavior.[4] At low temperatures, these blends are usually characterized by a positive Flory−Huggins interaction parameter, χ, indicative of repulsive interactions between the monomers. Upon heating, χ decreases. In some cases, however, homopolymer mixtures phase separate upon heating; i.e., they exhibit a lower critical solution temperature or LCST behavior.[4,5] At low temperatures, these blends are usually characterized by a negative χ parameter indicative of attractive interactions between the monomers. Upon heating, χ increases. In rare cases, temperature has a negligible effect on polymer blend thermodynamics; i.e., χ is a very weak function of temperature. The temperature-independent contribution to the Flory−Huggins interaction parameter is often called the "entropic" contribution, and we thus refer to these kinds of blends as entropic blends. It should be noted that in the conventional Flory−Huggins theory the interaction energy and entropic contributions to mixing are independent of temperature. The temperature dependence of χ arises due to the relative importance of these contributions at finite temperatures. Entropy dominates at high temperatures while energy dominates at low temperatures.[1,2]

Relatively few experimenters have examined the effect of pressure on the thermodynamics of polymer mixtures.[6−25] Qualitatively different behaviors are seen in UCST and LCST blends. Increasing pressure induces demixing in UCST systems and mixing in LCST systems. We argue that this is due to differences in the volume change of mixing.[14,25,26] The average monomer−monomer distance in UCST mixtures is expected to be somewhat larger than in the pure components due to repulsive interactions; i.e., the volume change of mixing ΔV is positive. In contrast, the average monomer−monomer distance in LCST mixtures is somewhat smaller than in the pure components due to attractive interactions; i.e., ΔV is negative. This leads to a $P\Delta V$ contribution to the Gibbs free energy change of mixing, ΔG, which is positive in the case of UCST systems and negative in the case of LCST systems. On the basis of these arguments, one might conclude that the thermodynamic properties of entropic blends would be independent of pressure. We note that the expected behavior is not always observed; for example, it was reported previously that pressure induces mixing in a diblock copolymer with a UODT (upper order−disorder transition).[27] Independent measurements of ΔV are needed to fully understand the underpinnings of pressure-dependent phase behavior.

The purpose of this paper is to study the effect of pressure on a multicomponent polymer blend wherein all three kinds of interactions described above are present. The blend of interest is a mixture of two homopolymers A and B and an A−C diblock copolymer. At atmospheric pressure, binary A/C mixtures exhibit UCST behavior, binary B/C mixtures exhibit LCST behavior, and binary A/B mixtures exhibit entropic behavior

[†] Department of Chemical Engineering, UC Berkeley.
[‡] Earth Science Division, UC Berkeley.
[§] Materials Sciences Division and Environmental Energy Technologies Division, UC Berkeley.
[||] ExxonMobil Research and Engineering.
[⊥] University of Houston.
[#] Present address: NIST Center for Neutron Research, National Institute of Standards and Technology, Gaithersburg, MD 20899.

10.1021/ma061894w CCC: $37.00 © 2007 American Chemical Society
Published on Web 12/21/2006

with a slight tendency toward LCST behavior. We note in passing that proving that a blend is perfectly entropic, i.e., one wherein the thermodynamic properties are truly independent of temperature, is impossible due to finite experimental uncertainty in the measured data. Our interest in these mixtures stems from previous studies where it has been shown that A−C diblock copolymers are effective surfactants for organizing mixtures of immiscible A and B homopolymers.[28−35] The thermodynamic properties of our A−C surfactants are similar to those of nonionic surfactants (alkyl polyglycol ether molecules) in oil/water systems at atmospheric pressure.[36−41] In the small molecule system, A is alkane, B is water, and C is polyglycol ether. In both the polymeric and aqueous systems, the A−C surfactant is designed such that the C part has attractive interactions with component B and repulsive interactions with component A at atmospheric pressure. The A−C surfactant design differs from the more common approach of using an A−B diblock copolymer to organize A and B homopolyers.[42−46] In the A/B/A−B system, there is only one parameter, χ_{AB}. In contrast, the thermodynamics of A/B/A−C blends are governed by three Flory−Huggins interaction parameters, χ_{AB}, χ_{AC}, and χ_{BC}.

The effect of pressure on oil/water/surfactant systems has been studied by several authors.[47−62] In mixtures containing nonionic surfactants,[47−55] it was found that increasing the pressure increased the LCST of water/nonionic surfactant mixtures, i.e., pressure-induced mixing. Increasing the pressure increases the UCST in oil/nonionic surfactant mixtures; i.e., pressure induces demixing. The behavior of surfactant/water and surfactant/oil mixtures is thus consistent with the ΔV-based arguments given above. The competition between these two opposing effects leads to interesting changes in the phase behavior of oil/water/surfactant mixtures at elevated pressures.[47] One observation that was made was that, in starting with a two-phase oil/water/nonionic surfactant mixture in which the surfactant was primarily soluble in the oil-rich phase, two phase transitions occurred with increasing pressure at constant temperature. The first transition resulted in the formation of a three-phase system which then gave way to a new two-phase system with the surfactant located primarily in the water-rich phase. The transfer of the surfactant from the oil to the water phase can be anticipated from the binary surfactant/water and surfactant/oil results described above due to changes in surfactant solubility with pressure.[47,48,50−53] Decreasing temperature (at constant pressure) leads to the same sequence of phase transitions. In addition, the three-phase region widens and moves to higher temperatures with increasing pressure.[47−49] Therefore, a system that does not exhibit a three-phase region at atmospheric pressure may exhibit a three-phase region at elevated pressures, as shown in ref 48.

In our polymeric A/B/A−C mixtures all of the components are saturated hydrocarbons with empirical formula CH_2. Component A is a saturated polybutadiene with 89% 1,2-addition (sPB89), component B is polyisobutylene (PIB), and the diblock copolymer (A−C) consists of block A (also sPB89) and block C which is a saturated polybutadiene with 63% 1,2-addition (sPB63). The prefix "s" stands for "saturated" and is replaced by "h" or "d" when we wish to specify whether the polymer is hydrogenated or deuterated. All of our conclusions regarding phase behavior are based on small-angle neutron scattering (SANS). At atmospheric pressure, χ_{AB} is a very weak function of temperature and thus falls under the category of an entropic system. χ_{AC} is positive at low temperatures and decreases with increasing temperature and is thus a UCST system. χ_{BC} is negative at low temperatures and increases with increasing temperature and is thus a LCST system. At atmospheric pressure, our A/B/A−C blend formed a lamellar phase at low temperatures, a microemulsion at intermediate temperatures, and a macrophase-separated state at high temperatures.[29] At elevated pressures, however, we observed a large window where a homogeneous phase was obtained. This was an unexpected result, as the atmospheric pressure data contained no hint of a homogeneous phase. This result is also very different from that obtained from pressurized oil/water/surfactant mixtures described above. In an attempt to understand the underpinnings of this behavior, we measured the pressure dependencies of χ_{AB}, χ_{AC}, and χ_{BC} in the polymeric system. The χ_{BC} data were in agreement with data obtained from other LCST systems described above. χ_{AC} was independent of pressure over the limited pressure range where we were able to obtain the data. The pressure dependence of χ_{AB}, the entropic system, was completely unexpected, as χ_{AB} decreased as the pressure increased. We use mean-field theories [Flory−Huggins theory (FHT), the random phase approximation (RPA), and self-consistent-field theory (SCFT)] with the measured pressure and temperature dependencies of χ_{AB}, χ_{AC}, and χ_{BC} to predict the phase behavior of our A/B/A−C mixture. The applicability of mean-field theories to high-pressure thermodynamic data is discussed in refs 14 and 25. The pressure and temperature dependencies of all of the parameters needed to complete the theoretical calculations—the volume of a repeat unit of each component, $v_m(P,T)$, binary interactions parameters, $\chi_{mn}(P,T)$, and the statistical segment lengths of each component, $l_m(P,T)$—were obtained from independent measurements. We can thus compare theoretical predictions and experimental results without resorting to any adjustable parameters.

While our study is primarily motivated by fundamental questions about the dependence of the phase behavior of multicomponent polymer blends on pressure, our results are relevant to polymer processing applications such as extrusion and injection molding wherein polymer mixtures are subjected to high pressures.

Experimental Methods

In the A/B/A−C polymer blends, component A was saturated polybutadiene with 89% 1,2-addition (sPB89), component B was polyisobutylene (PIB), and component C was saturated polybutadiene with 63% 1,2-addition (sPB63) (the prefix "s" stands for "saturated" and is replaced by "h" or "d" when we wish to specify whether the polymer is hydrogenated or deuterated).

Polybutadiene homopolymers and diblock copolymers were synthesized via anionic polymerization, and the C=C double bonds were saturated with hydrogen or deuterium gas per methods described in refs 29 and 34. Polyisobutylene was synthesized via cationic polymerization, also described in refs 29 and 34.

All saturated polybutadiene and polyisobutylene polymers were characterized using known methods[29] to determine the density, the weight-average molecular weight, polydispersity index, and % 1,2-addition (for the saturated polybutadiene polymers). The characterization parameters are summarized in Table 1 for the polymers used in this study. The composition labels for our samples are based on our targets. Samples wherein the % 1,2-addition deviated more than 3% from the target were discarded.

The pressure and temperature dependencies of the volume of a monomer unit, $v_{mon,m}$, for each type of polymer were measured by Krishnamoorti.[63] The Tait equation was used to describe the pressure and temperature dependencies of $v_{mon,m}$:

$$v_{mon,m} = V_{0,m}\exp(\alpha_m T)\left[1 - 0.0894\ln\left(1 + \frac{P}{B_{0,m}\exp(-B_{1,m}T)}\right)\right] \quad (1)$$

Table 1. Characterization of Polymers[a]

name	M_w (kg/mol)	N	PDI	ρ (g/mL)	% 1,2-addition	n_D
hPB89(10)	10.1	195	1.01	0.8625	89.1	NA
dPB89(10)	10.6	195	1.01	0.9020	89.1	2.54
dPB63(10)	10.5	191	1.02	0.9125	61.6	3.44
dPB89(35)	36.5	671	1.02	0.9037	90.1	2.56
PIB(13)	12.5	227	1.04	0.9134	NA	NA
PIB(45)	44.6	811	1.04	0.9140	NA	NA
hPBPB(41−38)	41.3−37.6	794−727	1.01	0.8633	91.9−62.7	NA

[a] M_w is the weight-averaged molecular weight, PDI is the polydispersity index, N is the number of reference volume units per chain at 23 °C based on a reference volume of 0.1 nm^3, PDI = M_w/M_n where M_n is the number-average molecular weight, ρ is the average density, and n_D is the number of deuterium atoms per C_4 repeat unit.

Table 2. Parameters for the Tait Equation

polymer	$V_{0,m}$	α_m	$B_{0,m}$	$B_{1,m}$
sPB89 (polymer A)	86.50	0.000 723 9	6.498	0.004 681
sPB63 (polymer C)	86.33	0.000 732 1	6.786	0.004 717
PIB (polymer B)	86.23	0.000 566 4	7.252	0.004 023

where $V_{0,m}$, α_m, $B_{0,m}$, and $B_{1,m}$ are parameters determined from fitting the Tait equation to the data and are listed in Table 2.

Binary and multicomponent polymer blends were created via methods described in ref 29. The samples were annealed inside a Teflon O-ring on a piece of Teflon at 90 °C for 2 days to ensure complete removal of the solvent used in the blend preparation.

Small-angle neutron scattering (SANS) experiments were conducted on the NG7 beamline at the National Institute of Standards and Technology in Gaithersburg, MD.[64] Using standard procedures, raw data were converted to absolute coherent scattering intensity, I, as a function of q ($q = 4\pi \sin(\theta/2)/\lambda$, θ is the scattering angle, λ is the wavelength of the incident beam), after corrections for detector sensitivity, background, empty cell, and incoherent scattering were made, using standard procedures.[65] For the deuterated components, corrections for the nonuniformity of deuterium labeling were made.[66] The sample was placed between two sapphire windows in the NIST pressure cell and pressurized using the experimental setup and methods described in ref 14. The SANS data are limited to $q < 0.5$ nm^{-1} due to the physical design of the pressure cell. The upper temperature limit was 200 °C. The pressure range for the cell was 0.03−3.10 kbar. In our previous studies on high molecular weight polyethylbutylene and polymethylbutylene, we were able to access the entire temperature and pressure range. In the present work, however, some of the blends leaked out of the pressure cell at pressures well below 3.10 kbar. This problem seemed to depend on the viscosity of the blend: samples with lower viscosity leaked out at lower temperatures and pressures than samples with higher viscosities. Despite many separate attempts, we were unable to solve this problem. The pressure and temperature ranges over which blends discussed in this paper were studied was limited by this fact. All of the blends discussed in this paper were studied at atmospheric pressure in ref 29. All of the plots contain two data points in the vicinity of $P \cong 0$: one from the present study and the other from ref 29.

Definitions and Theory

We use a reference volume $\upsilon = 0.1$ nm^3, which is roughly the volume of a C_4 repeat unit of our components, as the basis for defining the following parameters: the Flory−Huggins interaction parameters χ_{mn} (m, n = A, B, C), the number of reference volume units per chain of each component (N_j), and the statistical segment length of each component (l_m), which describe the dependencies of the radius of gyration on N_j. Since the polymer density is temperature dependent, N_j is also temperature dependent.

Our methods for utilizing Flory−Huggins theory (FHT),[67,68] the random phase approximation (RPA),[69−71] and self-consistent-field theory (SCFT)[31,72−75] to describe multicomponent A/B/A−C blends have been previously discussed in refs 29 and 34. The only input parameters (in addition to usual characterization parameters such as molecular weight and the volume of a repeat unit) needed to utilize these theories are the χ_{mn} for each pair and l_m parameters for each component, which are determined from binary blends. Our SCFT calculations are carried out in 1 dimension, and the effect of concentration fluctuations is neglected. We thus do not differentiate between different microphase separated states such as microemulsions and lamellae. Our analysis does not consider that the χ parameter often also accounts for other effects such as local entropic packing contributions, compressibilities, molecular volume differences, etc.

Table 3. Compositions of Binary Blends Used To Measure χ

blend	component A	component B	component C	ϕ_A	ϕ_B	ϕ_C
B1	dPB89(10)	PIB(45)		0.673	0.327	
B2	hPB89(10)		dPB63(10)	0.493		0.507
B3		PIB(13)	dPB63(10)		0.477	0.523

Binary Interaction Parameters at Elevated Pressures

The SANS profiles were measured from three binary blends, A/B, A/C, and B/C (blends B1, B2, and B3, respectively, described in Table 3), at a variety of temperatures and pressures. Figure 1 shows data obtained from all three blends at 30 °C at selected pressures. The RPA was fit to the data with χ_{mn} as a fitting parameter. Previously, we determined that the statistical segment length based upon the C_4 repeat unit volume, $l_{mon,m} = l_m\sqrt{\upsilon_{mon,m}/\upsilon}$, where $\upsilon_{mon,m}$ is the monomer volume based on a C_4 repeat unit, is independent of temperature at atmospheric pressure.[29,34] In this work, we assume that $l_{mon,m}$ are also independent of pressure. We were unable to substantiate the limitations of this assumption due to the limited q range accessible with the NIST pressure cell. However, all of the data obtained from the binary blends are consistent with this simplifying assumption; i.e., the experimental data could be fit with χ_{mn} as the only adjustable parameter. We will use the statistical segment lengths reported in ref 34 at all temperatures and pressures: $l_{mon,A} = 0.55$ nm, $l_{mon,B} = 0.58$ nm, and $l_{mon,C} = 0.75$ nm.

The results of fitting the RPA equation to the SANS data of A/B, B/C, and A/C blends at 30 °C using χ_{mn} as fitting parameters give the solid curves shown in Figure 1. This was also done for other temperatures, and the data will not be shown for brevity. The χ_{mn} parameters obtained from these fits are shown in Figure 2, in which χ_{mn} are plotted as a function of inverse temperature at each pressure. In Figure 3, χ_{mn} are plotted as a function of pressure at each temperature. The A/B blend exhibited a positive parameter at atmospheric pressure that was fairly temperature independent.[34] There is the slightest hint of LCST behavior at atmospheric pressure. However, upon pressurization, χ_{AB} was found to decrease drastically. This is true for all pressures. As the pressure is increased, the LCST behavior of the A/B blend becomes much more pronounced (Figures 2a and 3a). These data lead to the surprising conclusion that sPB89/

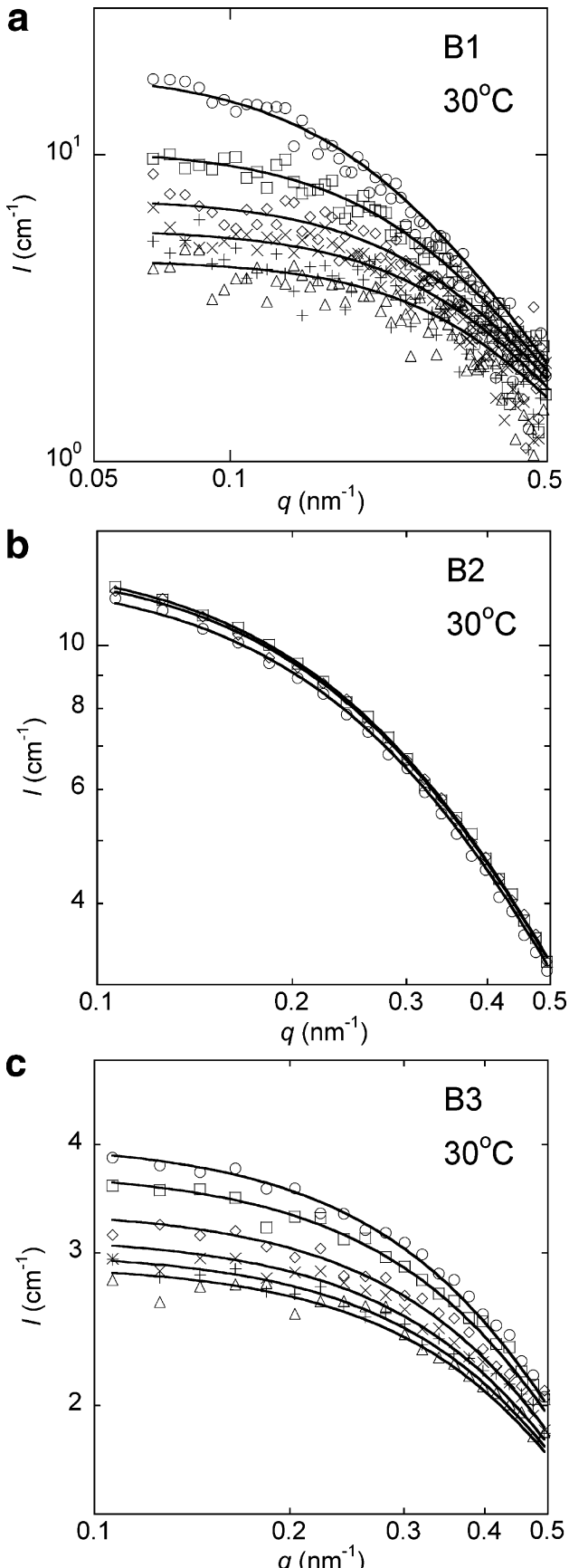

Figure 1. SANS at 30 °C from (a) blend B1 (A/B), (b) blend B2 (A/C), and (c) blend B3 (B/C) at selected pressures. The solid lines are the random phase approximation fit to the data with χ_{mn} as an adjustable parameter and with $l_{\mathrm{mon},m}$ constrained to a temperature- and pressure-independent value. (a, c) Data markers: 0.03 (○), 0.62 (□), 1.24 (◇), 1.86 (×), 2.48 (+), and 3.10 kbar (△). (b) Data markers: 0.03 (○), 0.34 (□), and 0.69 kbar (◇).

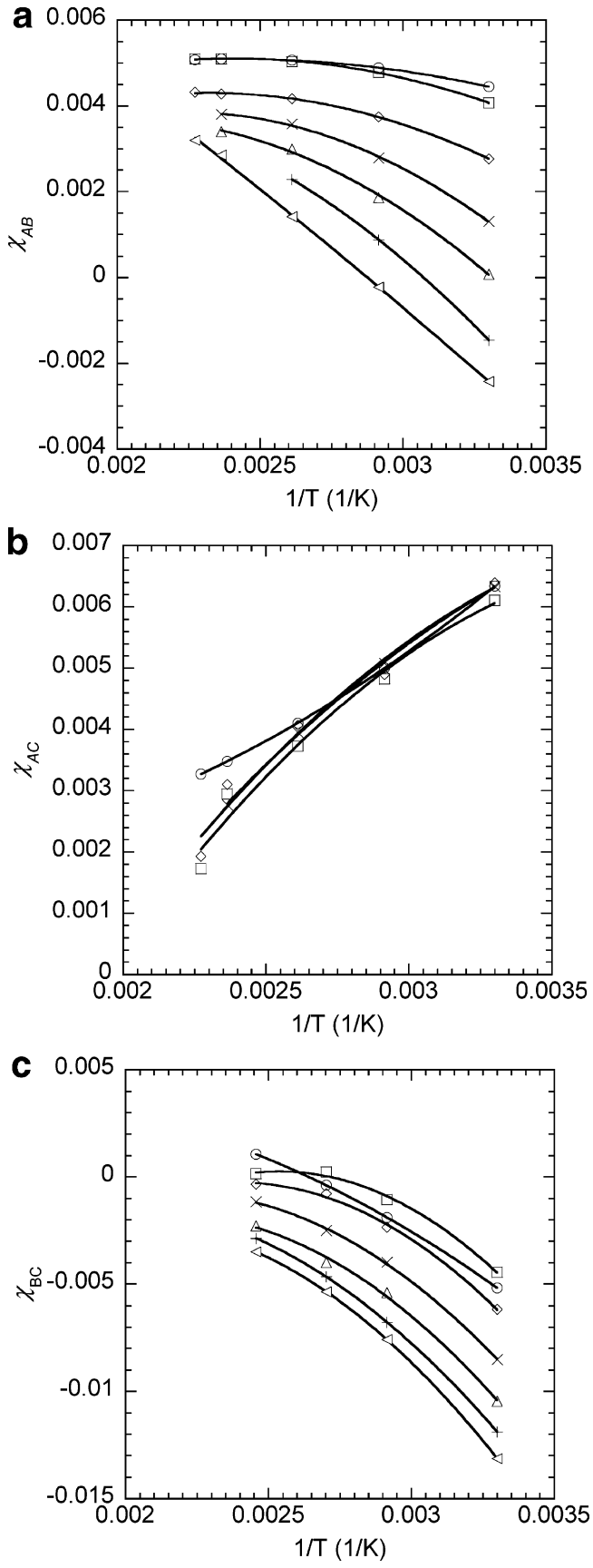

Figure 2. χ parameters as a function of $1/T$ obtained from RPA fits for the (a) A/B, (b) A/C, and (c) B/C blends. Fit to the expression $\chi = A + BT^{-1} + CT^{-2}$ are shown as the solid curves in Figure 2. (a, c) Data markers: atmospheric pressure (from ref 34) (○), 0.03 (□), 0.62 (◇), 1.24 (×), 1.86 (△), 2.48 (+), and 3.10 kbar (left facing △). (b) Data markers: atmospheric pressure (from ref 34) (○), 0.03 (□), 0.34 (◇), and 0.69 kbar (×).

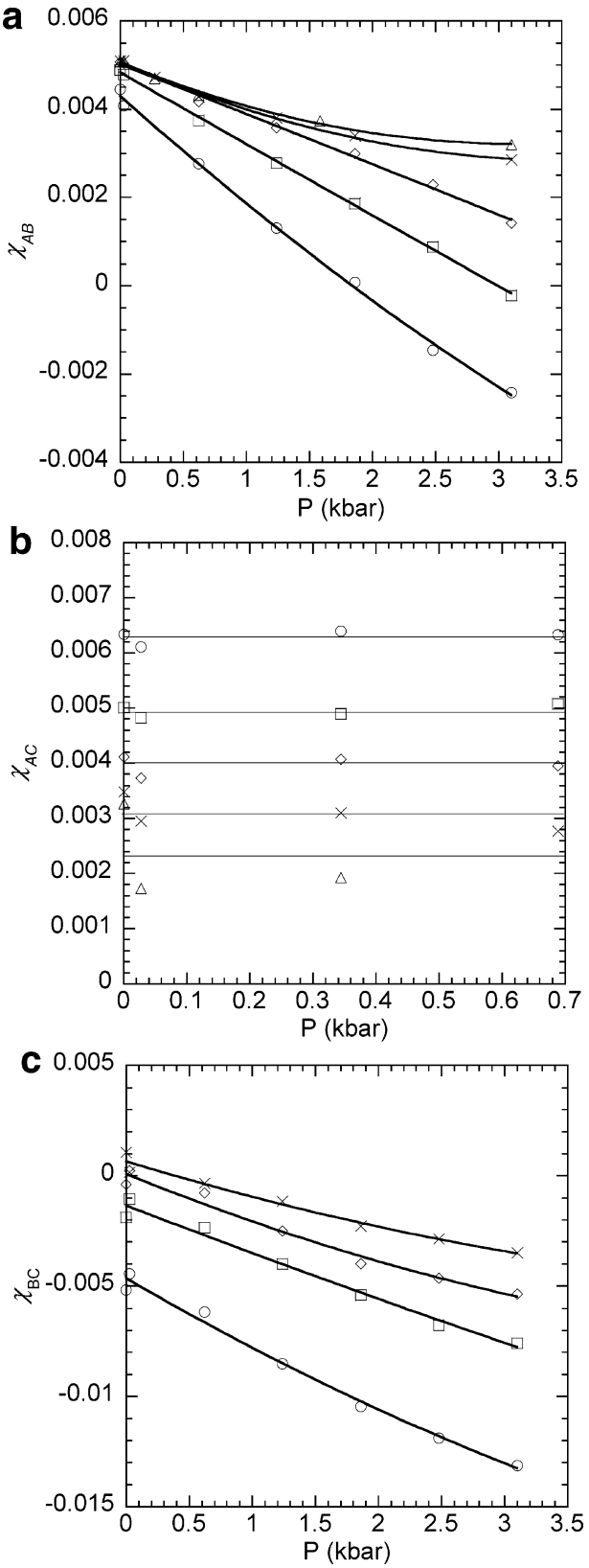

Figure 3. χ parameters as a function of P obtained from RPA fits for the (a) A/B, (b) A/C, and (c) B/C blends. Fit to the expression $\chi = D + EP + FP^2$ are shown as solid curves. Data are also included at atmospheric pressure, as described in ref 34. (a, b) Data markers: 30 (○), 70 (□), 110 (◇), 150 (×), and 167 °C (Δ). (c) Data markers: 30 (○), 70 (□), 97 (◇), and 134 °C (×).

PIB blends would be miscible with each other at room temperature and 3.10 kbar, regardless of the molecular weight of the components. The thermodynamics of polyolefin mixtures has been studied extensively.[76−79] The results presented in Figures 2a and 3a could not be anticipated from this extensive body of work. It is clear from this study that the "term" entropic blend is probably not appropriate for blends that show temperature-independent χ parameters at atmospheric pressure.

Table 4. Polynomial Constants for Parameters Determined from Binary Blends[a]

χ_{AB}

P (kbar)	A	B (K)	C (K^2)
0.03	-2.28×10^{-3}	6.14×10^{0}	-1.28×10^{3}
0.62	-4.34×10^{-3}	7.45×10^{0}	-1.60×10^{3}
1.24	-7.69×10^{-3}	1.03×10^{1}	-2.29×10^{3}
1.86	-5.42×10^{-3}	9.00×10^{0}	-2.22×10^{3}
2.48	-1.64×10^{-3}	7.00×10^{0}	-2.10×10^{3}
3.10	1.36×10^{-2}	-3.85×10^{0}	-3.01×10^{2}
T (°C)	D	E (kbar^{-1})	F (kbar^{-2})
30	4.30×10^{-3}	-2.56×10^{-3}	1.18×10^{-4}
70	4.83×10^{-3}	-1.63×10^{-3}	5.29×10^{-6}
110	5.01×10^{-3}	-1.12×10^{-3}	-5.71×10^{-6}
150	5.07×10^{-3}	-1.26×10^{-3}	1.76×10^{-4}
167	5.06×10^{-3}	-1.18×10^{-3}	1.87×10^{-4}

χ_{BC}

P (kbar)	A	B (K)	C (K^2)
0.03	-5.23×10^{-2}	4.14×10^{1}	-8.16×10^{3}
0.62	-4.18×10^{-2}	3.47×10^{1}	-7.24×10^{3}
1.24	-3.04×10^{-2}	2.71×10^{1}	-6.23×10^{3}
1.86	-3.18×10^{-2}	2.80×10^{1}	-6.52×10^{3}
2.48	-2.23×10^{-2}	2.18×10^{1}	-5.64×10^{3}
3.10	-2.79×10^{-2}	2.58×10^{1}	-6.47×10^{3}
T (°C)	D	E (kbar^{-1})	F (kbar^{-2})
30	-4.65×10^{-3}	-3.33×10^{-3}	1.76×10^{-4}
70	-1.35×10^{-3}	-2.20×10^{-3}	4.13×10^{-5}
97	8.03×10^{-5}	-2.33×10^{-3}	1.71×10^{-4}
134	6.49×10^{-4}	-1.73×10^{-3}	1.24×10^{-4}

χ_{AC}

P (kbar)	A	B (K)	C (K^2)
all[b]	-1.25×10^{-2}	8.57×10^{0}	-8.77×10^{2}

[a] At each pressure $\chi_{mn} = A + BT^{-1} + CT^{-2}$, and at each temperature $\chi_{mn} = D + EP + FP^2$. [b] χ_{AC} was not a strong function of pressure, and thus the average values at each temperature were fit to $\chi_{AC} = A + BT^{-1} + CT^{-2}$.

At atmospheric pressure, χ_{AC} was positive at room temperature and decreased with increasing temperature.[34] Over the limited accessible pressure range (only $P < 0.69$ kbar could be accessed due to sample leakage), the change in χ_{AC} upon pressurization was negligible as shown in Figures 2b and 3b. At atmospheric pressure, χ_{BC} was negative and increased with increasing temperature.[34] χ_{BC} was found to decrease with increasing pressure, consistent with the ΔV-based arguments presented in the Introduction (Figures 2c and 3c). χ_{BC} could only be measured up to $T = 134$ °C due to sample leakage at higher temperatures.

The χ_{AB} and χ_{BC} parameters were fit at each pressure to an equation of the form $\chi_{mn} = A + BT^{-1} + CT^{-2}$ (solid curves in Figure 2), and the A, B, and C parameters for each blend at each pressure are listed in Table 4. In addition, the χ_{AB} and χ_{BC} parameters were fit at each temperature to an equation of the form $\chi_{mn} = D + EP + FP^2$ (solid curves in Figure 3), and the D, E, and F parameters for each blend at each temperature are listed in Table 4. With these sets of equations, the parameters can be determined at any pressure and temperature.[80] χ_{AC} was insensitive to pressure in the available pressure window. Thus, the average values of χ_{AC}, calculated at each temperature (over

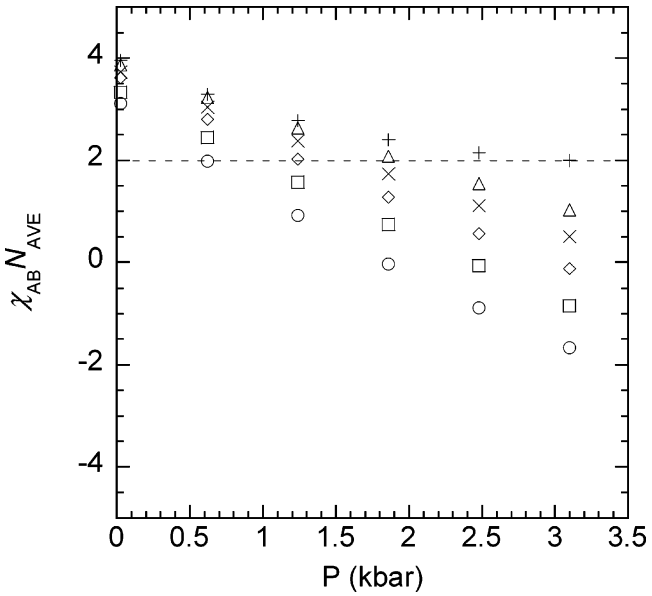

Figure 4. $\chi_{AB}N_{AVE}$ as a function of pressure at the following temperatures: 30 (○), 50 (□), 70 (◇), 90 (×), 110 (△), and 130 °C (+). Dotted line indicates location of $\chi_{AB}N_{AVE} = 2.0$.

the pressure range of atmospheric pressure to 0.69 kbar), were fit to the form $\chi_{mn} = A + BT^{-1} + CT^{-2}$. The values of *A*, *B*, and *C* thus obtained are listed in Table 4. We have implicitly assumed that χ_{AC} is independent of pressure up to 3.10 kbar although our data are restricted to $P < 0.69$ kbar.

Multicomponent A/B/A−C Blend at Elevated Pressures

We conducted SANS experiments at a variety of temperatures and pressures on a multicomponent A/B/A−C blend, labeled blend B50, with the following components: A was dPB89(35), B was PIB(45), and the A−C diblock copolymer was hPBPB(41−38). The characteristics of all of these polymers are given in Table 1. The ratio of the volume fractions of the A and B homopolymers in the multicomponent blend are at their critical composition: $\phi_A/\phi_B = 1.114 \pm 0.002$. The composition of blend B50 is $\phi_A = 0.264$, $\phi_B = 0.237$, and $\phi_{A-C} = 0.500$.

Before examining the phase behavior of the multicomponent blend, it is useful to evaluate the properties of the dPB89(35)/PIB(45) blend in the absence of the A−C surfactant. We do this by examining the value of $\chi_{AB}N_{AVE}$, where

$$1/N_{AVE} = [1/(2N_A^{1/2}) + 1/(2N_B^{1/2})]^2 \qquad (2)$$

In a critical A/B blend, phase separation is obtained when $\chi_{AB}N_{AVE}$ is greater than 2.0. The temperature and pressure dependencies of $\chi_{AB}N_{AVE}$ for dPB89(35)/PIB(45) are given in Figure 4. It is clear from Figure 4 that there are many values of *T* and *P* where $\chi_{AB}N_{AVE}$ is less than 2.0, implying that a critical A/B blend would be homogeneous in the absence of the A−C surfactant. It is highly unlikely that the addition of the surfactant to these blends would change the homogeneous nature of the blend ($\chi_{AC}N_{AVE}$ for the A and C blocks of the diblock copolymer is <10.5 across the entire range of temperatures and pressures). We thus expect the A/B/A−C blend to be homogeneous at *T*, *P* values where $\chi_{AB}N_{AVE}$ is significantly less than 2.0, which generally occurs at elevated pressures.

The phase behavior at atmospheric pressure of blend B50 has been fully analyzed in ref 29 and will only be summarized here. At atmospheric pressure, blend B50 is lamellar at 30 °C, a microemulsion at temperatures between 70 and 90 °C, and macrophase separated above 112 °C. The state of blend B50 at atmospheric pressure and 50 °C had characteristics of both lamellar phases and microemulsions. It is possible that lamellae and microemulsions coexist at temperatures between 30 and 70 °C, as required by the Gibbs phase rule.[29]

We begin with the data obtained from blend B50 at $T = 30$ °C and $P = 0.03-3.10$ kbar, shown in Figure 5a. We see a single scattering peak in the vicinity of $q = 0.135$ nm^{-1} at all pressures. This scattering peak could either imply the presence of a homogeneous phase with periodic concentration fluctuations or the presence of a microphase separated blend without significant long-range order. As we have done in ref 34, we use RPA, SCFT, and FHT along with the measured SANS data to distinguish between these two possibilities. We expect a homogeneous phase at high pressures where $\chi_{AB}N_{AVE}$ is significantly less than 2.0 (see Figure 4). We thus used multicomponent RPA to compute the SANS intensity of B50 at $T = 30$ °C and elevated pressures. Our methods for utilizing the multicomponent RPA are described in detail in refs 29 and 34. As we use binary χ_{mn} and l_m parameters, there are no fitting parameters in the theoretical calculations. In Figure 5b we compare the RPA predictions with experimental data at $P \geq 2.48$ kbar. Many features seen in the experiments are accurately captured by RPA. Both theory and experiment indicate a plateau in *I* of 30−40 cm^{-1} as $q \rightarrow 0$, the presence of a scattering peak due to periodic concentration fluctuations, and a q^{-2} tail at high *q*. The peak location predicted by RPA occurs at $q = 0.15$ nm^{-1}, which is somewhat higher than that obtained experimentally. This is probably due to chain stretching in the multicomponent blend. We note in passing that in most cases statistical segment lengths obtained from homopolymer blends are significantly smaller than those obtained from neat diblock copolymers.[81] In addition, the theoretically predicted peak intensity at $P = 3.10$ kbar is lower by a factor of 2 when compared with experiment. This discrepancy may be due to uncertainties in measurement of χ_{mn}, l_m, and N_j or fluctuation effects that are not included in our theoretical calculations. Below 2.48 kbar, the calculated RPA profiles contain two poles, a signature of microphase separation (inset in Figure 5b shows $I(q)$ calculations for $P = 1.86$ kbar).

We use SCFT to study the state of the blend at $T = 30$ °C and pressures between 0.03 and 3.10 kbar. Our methods for utilizing SCFT to describe A/B/A−C blends have been previously discussed in refs 29 and 34. The SCFT calculations are based on the same binary χ_{mn} and l_m parameters that were used in the RPA calculations. The SCFT calculations predict the domain spacing, *d*, and the composition of the microphases. The dashed line in Figure 5c shows the calculated domain spacing as a function of *P* at $T = 30$ °C. The solid curve in Figure 5c is $d_{RPA} = 2\pi/q_{RPA-peak}$, where $q_{RPA-peak}$ is the location of the peak predicted by the RPA. The symbols in Figure 5c represent the experimentally determined domain spacing, $d_{expt} = 2\pi/q_{SANS-peak}$ where $q_{SANS-peak}$ is the location of the primary scattering peak measured with SANS. The pressure dependence of domain spacing is in excellent agreement with the predictions of RPA and SCFT. At $P \geq 2.48$ kbar, where RPA calculations gave $I(q)$ profiles without singularities, SCFT calculations converged on a homogeneous phase. The RPA and SCFT calculations are thus entirely consistent with each other.

The final calculation that we conducted was to utilize Flory−Huggins theory (FHT) to predict the dimensionless free energy of a homogeneous state, $(fv/kT)_{homog}$. The same binary χ_{mn} and l_m parameters used in the RPA and SCFT calculations are used in the FHT calculations, as described in detail in ref 34. This is then compared to the dimensionless free energy of the microphase separated state that was calculated with SCFT,

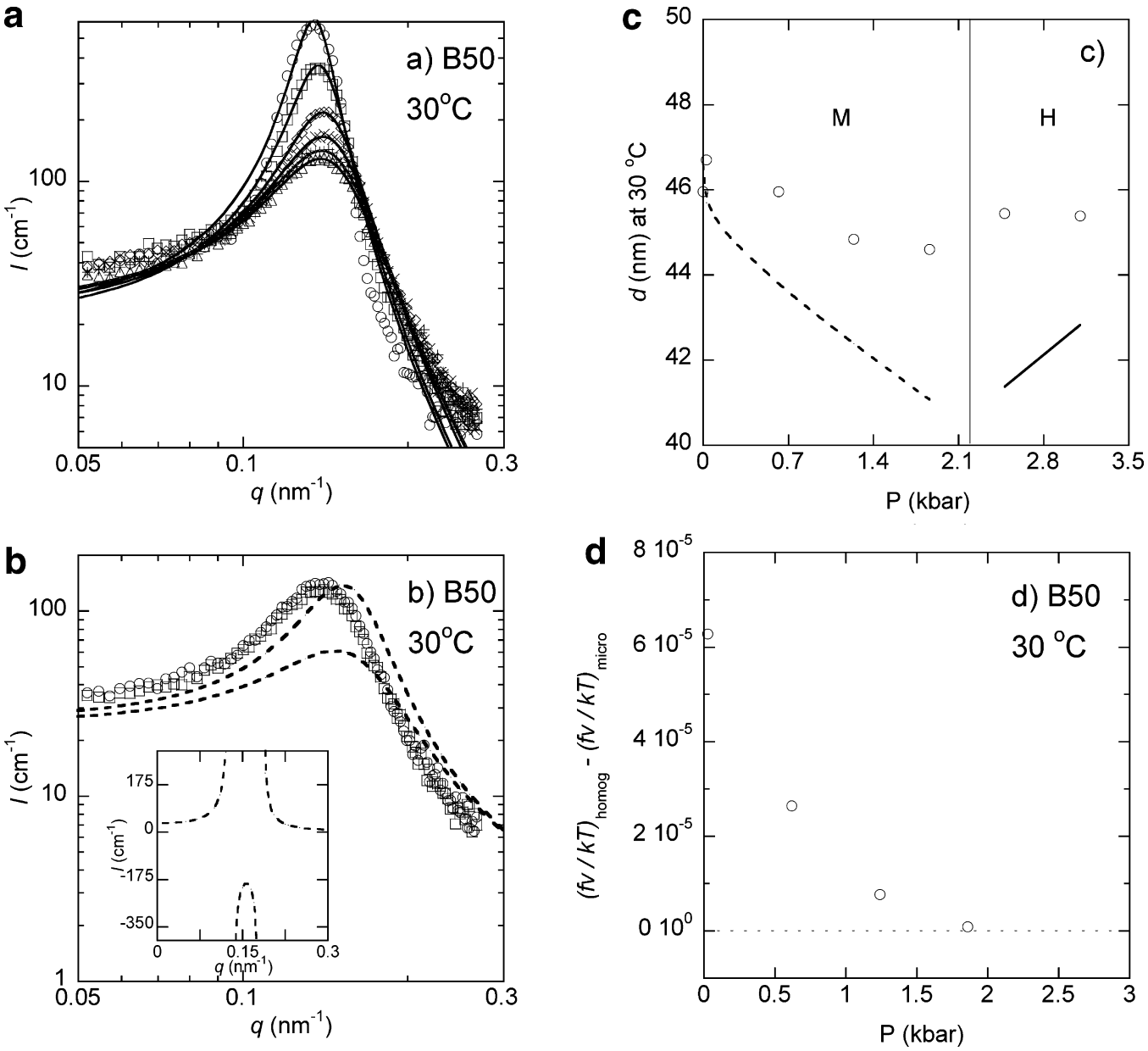

Figure 5. (a) SANS data obtained from blend B50 at 30 °C at selected pressures: 0.03 (○), 0.62 (□), 1.24 (◊), 1.86 (×), 2.48 (+), and 3.10 kbar (Δ). The solid lines are the T−S fit to the data. (b) SANS data obtained from blend B50 at 30 °C at selected pressures: 2.48 (○) and 3.10 kbar (□). The dotted curves are the RPA predictions with no adjustable parameters at $P = 2.48$ and 3.10 kbar (the peak intensity decreases as P increases). Inset to (b) is the RPA profile at 30 °C and 1.86 kbar with no adjustable parameters. (c) Domain spacing as a function of temperature for blend B50 at 30 °C as determined by SANS with $d = 2\pi/q_{SANS-peak}$ (○) and predicted by SCFT (dotted line) and the RPA (solid line). The vertical line indicates the MH phase boundary determined from SCFT, FHT, and RPA. M is microphase separated (lamellae or a microemulsion), and H is homogeneous. (d) Dimensionless free energy of the lamellar phase (predicted by SCFT) subtracted from dimensionless free energy of the homogeneous phase (predicted by FHT) as a function of pressure for B50 at 30 °C. Dotted line indicates $\Delta f = 0$.

$(fv/kT)_{micro}$. The free energies of the homogeneous and microphase separated states are very similar. We thus plot the dimensionless difference, $[(fv/kT)_{homog} - (fv/kT)_{micro}]$, as a function of pressure at 30 °C in Figure 5d. As evidenced in Figure 5d, the free energy of the microphase separated state is less than the free energy of the homogeneous phase at all pressures that SCFT converged on a d spacing ($P \leq 1.86$ kbar). This is in agreement with the RPA analysis which predicted microphase separation at P between 0.03 and 1.86 kbar and a homogeneous phase at $P \geq 2.48$ kbar. Utilizing SCFT, FHT, and RPA calculations, the theoretical transition from a microphase separated state to a homogeneous state occurs at $P = 2.15 \pm 0.05$ kbar.

To determine the nature of the microphase separated state, we analyze the SANS profile using the Teubner−Strey (T−S) equation.[82] Agreement with the T−S equation is taken as an indication of a microemulsion phase. The T−S equation for the scattering intensity is

$$I(q) = \frac{1}{a + bq^2 + cq^4} + I_{bgd}(q) \qquad (2)$$

where a, b, and c are fitting parameters. We use $I_{bgd}(q)$ to account for the fact the T−S equation was developed for oil/water microemulsions and thus does not account for scattering contributions due to the connectivity of polymer chains. $I_{bgd}(q)$ is assumed to be of the form $I_{bgd}(q) = (eq^2 + g)^{-1}$, where e and g are fitting constants. We do not have rigorous justification for the proposed splitting of $I(q)$. The use of the background term does not affect the resulting a, b, and c coefficients

Table 5. Teubner−Strey Fitting Parameters

T (°C)	P (kbar)	a (cm)	b (cm nm^2)	c (cm nm^4)	d (nm)	ξ (nm)	f_a
30	0.03	0.046 64	−4.952	136.20	46.39	78.30	−0.9824
30	0.62	0.048 52	−4.856	128.71	45.41	60.26	−0.9716
30	1.24	0.044 84	−4.101	104.53	44.25	42.72	−0.9471
30	1.86	0.042 27	−3.689	93.95	43.97	35.58	−0.9255
30	2.48	0.040 99	−3.490	89.81	43.99	32.15	−0.9094
30	3.10	0.041 79	−3.525	91.33	44.05	30.91	−0.9021
50	0.03	0.029 59	−3.062	89.05	47.21	43.93	−0.9432
50	0.62	0.033 33	−2.772	72.89	44.21	29.05	−0.8892
50	1.24	0.038 46	−2.589	64.94	42.23	21.32	−0.8192
50	1.86	0.041 48	−2.172	54.44	40.75	16.16	−0.7225
50	2.48	0.044 62	−1.996	51.65	40.26	14.09	−0.6573
50	3.10	0.044 83	−1.717	47.48	40.22	12.58	−0.5885
70	0.03	0.029 25	−2.817	86.62	47.74	30.73	−0.8848
70	0.62	0.037 52	−2.409	67.45	43.65	18.68	−0.7571
70	1.24	0.041 56	−1.786	50.05	41.14	13.50	−0.6190
70	1.86	0.047 40	−1.677	46.67	39.80	11.99	−0.5637
70	2.48	0.048 67	−1.137	35.76	38.68	9.76	−0.4308
70	3.10	0.052 86	−0.969	30.56	37.08	8.81	−0.3810
90	0.03	0.025 33	−2.175	80.97	50.37	21.68	−0.7594
90	0.62	0.041 00	−1.791	57.65	43.26	13.40	−0.5824
90	1.24	0.049 31	−1.402	44.15	40.02	10.68	−0.4750
90	1.86	0.053 78	−1.093	37.11	38.67	9.26	−0.3867
90	2.48	0.057 44	−0.943	32.84	37.49	8.53	−0.3432
90	3.10	0.062 39	−0.804	28.54	36.03	7.82	−0.3012

significantly, as the background term is only important at high q values (away from the peak). The fitting constants enable determination of the domain spacing, d, correlation length, ξ, and amphiphilicity factor, f_a, given by

$$\xi = \left[\frac{1}{2}\left(\frac{a}{c}\right)^{1/2} + \frac{1}{4}\frac{b}{c}\right]^{-1/2} \tag{3}$$

$$d = 2\pi\left[\frac{1}{2}\left(\frac{a}{c}\right)^{1/2} - \frac{1}{4}\frac{b}{c}\right]^{-1/2} \tag{4}$$

$$f_a = \frac{b}{2\sqrt{ac}} \tag{5}$$

The T−S equation fit to the data at 30 °C is shown as the solid curves in Figure 5a. The fitting parameters are given in Table 5. The T−S equation captures all of the important features in the 30 °C $I(q)$ data, regardless of P. In the T−S equation, the parameter b must be negative if a peak is observed. As both a and c are positive for microemulsion formation, this results in a negative f_a. In our polymer systems, we observe homogeneous systems which exhibit a structure factor peak near the homogeneous-to-microphase separated state phase boundary. Therefore, homogeneous systems are observed with $f_a < 0$. For example, at $T = 30$ °C and $P = 2.48$ kbar the RPA predicts the existence of a homogeneous phase, and from the T−S fit, $f_a = -0.91$.

The combination of SANS, RPA, SCFT, and FHT indicates that at 30 °C blend B50 forms a microemulsion at $P \leq 1.86$ kbar and homogeneous at $P \geq 2.48$ kbar. The vertical line in Figure 5c demarcates the location of the homogeneous-to-microphase separation transition. We note that there are no discernible SANS signatures of this transition. Our theoretical analysis indicates that the microphase separated-to-homogeneous transition is a second-order phase transition because the free energy difference between the microphase separated state and the homogeneous state vanishes at the transition point (Figure 5d). This may be the reason for the lack of discernible experimental signatures of this transition. We note in passing that similar difficulties are faced when locating the transition distinguishing between homogeneous and microphase separated states in the microemulsion channel in well-studied A/B/A−B mixtures at atmospheric pressure.[83]

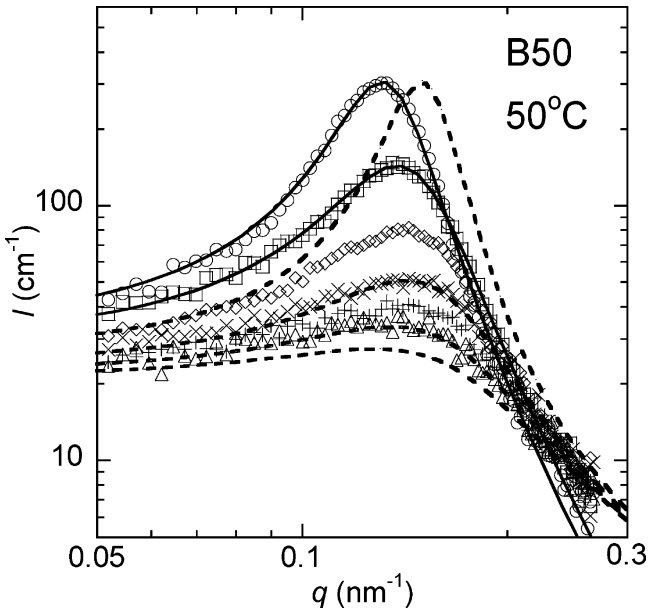

Figure 6. SANS data obtained from blend B50 at 50 °C at selected pressures: 0.03 (○), 0.62 (□), 1.24 (◊), 1.86 (×), 2.48 (+), and 3.10 kbar (Δ). The solid lines are the T−S fit to the data at $P = 0.03$ and 0.62 kbar. The dotted curves are the RPA predictions with no adjustable parameters at $P = 1.24$, 1.86, 2.48, and 3.10 kbar (the peak intensity decreases as P increases).

Table 6. Microphase Separated-to-Homogeneous Transition Pressures

T (°C)	P_{trans} (kbar)
30	2.15 ± 0.05
50	1.15 ± 0.05
70	0.56 ± 0.05
90	0.35 ± 0.05

Qualitatively similar behavior was seen in B50 at temperatures between 30 and 90 °C. The same methodology described above for the 30 °C data was applied to the data obtained at the other temperatures. In all cases, a microphase separated-to-homogeneous transition was obtained using SCFT, FHT, and RPA at pressures listed in Table 6. The results of the T−S analysis at these temperatures are given in Table 5. The SANS data obtained at 50 °C are shown in Figure 6. The solid curves represent T−S fits from microemulsion phases at $P = 0.03$−0.62 kbar. The dotted curves represent the RPA profiles at $P \geq 1.24$ kbar. As was the case at 30 °C, the scattering intensity predicted by RPA at $q \sim 0.14$ nm^{-1} diverges with decreasing pressure, announcing the formation of a microemulsion. The theoretically predicted RPA peak intensity overpredicts the peak intensity of the experimental profiles in the vicinity of the homogeneous-to-microphase separated phase transition (dotted curves in Figure 6). This may be due to uncertainties in measurement of χ_{mn}, l_m, and N_j or the lack of incorporation of fluctuation effects in the theory. The T−S equation was fit to all of the 50 °C data, and the fits are summarized in Table 5. The 70 and 90 °C data are not discussed here for brevity.

The data obtained from blend B50 at 130 °C are significantly different from those discussed thus far and are shown in Figure 7. This blend is macrophase separated at 0.03 kbar, as evidence by the low-q Porod $I \sim q^{-4}$ scattering profile observed due to the presence of large length scale structures (Figure 7). As the pressure is increased, the low-q Porod scattering disappears and the SANS profile is consistent with a homogeneous phase. The dashed curves in Figure 7 are RPA predictions with no adjustable parameters. The measured scattering profiles from the homogeneous phase do not contain a scattering peak,

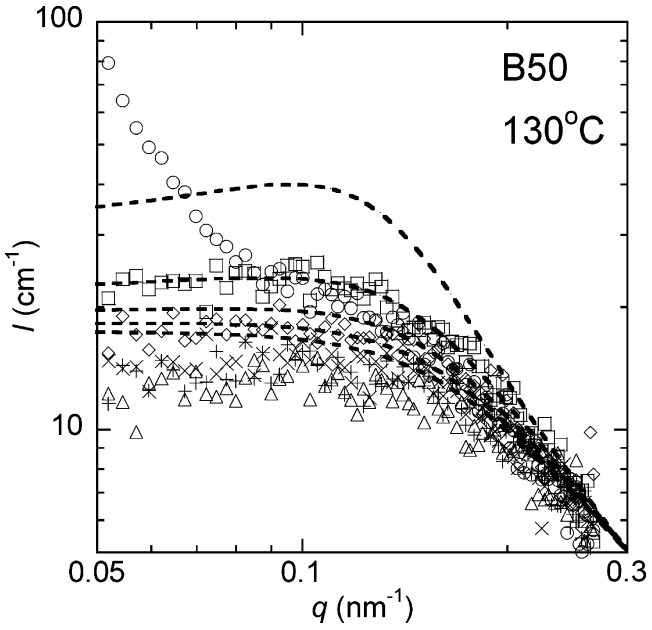

Figure 7. SANS data obtained from blend B50 at 130 °C at selected pressures: 0.03 (○), 0.62 (□), 1.24 (◊), 1.86 (×), 2.48 (+), and 3.10 kbar (Δ). The dotted curves are the RPA predictions with no adjustable parameters at $P = 0.62$, 1.24, 1.86, 2.48, and 3.10 kbar (the plateau intensity decreases as P increases).

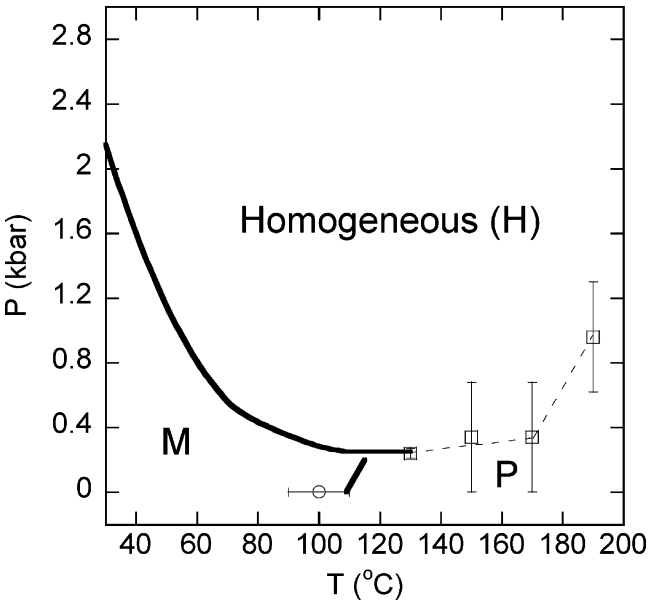

Figure 8. A/B/A−C phase diagram. M is microphase separated (lamellae or a microemulsion), H is homogeneous, and P is macrophase separated. The square and circle symbols show the P → H and M → P phase transitions, respectively, based upon the low-q scattering in the SANS data. The solid curves indicate the M → H, P → H, and M → P phase transitions based upon a combination of SCFT, RPA, and FHT. The dashed curve connects experimental data points. Errors on the theoretical transition pressures are 0.05 kbar for all phase boundaries.

irrespective of pressure. The RPA predictions capture this behavior. The quantitative differences between theory and experiment seen in Figure 7 is attributed to uncertainty in measurements of χ_{mn}, l_m, and N_j parameters, as fluctuation effects are typically more important near microphase separation and not macrophase separation.[84] It is relatively straightforward to identify the homogeneous-to-macrophase separation transition from the measurements due to the abrupt appearance of Porod scattering (Figure 7). At $T = 110$ °C and $P = 0.03$ kbar, an increase in the low-q scattering intensity indicates the presence of macrophase separation. We were not able to observe the $I \sim q^{-4}$ signature of macrophase separation. (At atmospheric pressure, the $I \sim q^{-4}$ profile was observed at 110 °C as the configuration used allowed access to lower q values.[29]) As the pressure was increased to 0.62 kbar, the profile was consistent with a homogeneous phase. We thus observe qualitatively similar behaviors at 110 and 130 °C. Data obtained at $T \geq 130$ °C were similar to the data described above for 130 °C. For brevity, we do not show these results.

Our experimental and theoretical results are summarized in the $T-P$ phase diagram shown in Figure 8. The symbols indicate the locations of the experimentally determined phase transitions. The square symbols show the homogeneous (H)-to-macrophase separation (P) phase transition, while the circle symbol shows the phase transition from a microphase separated state (M) to a macrophase separated state. The solid curves indicate the M → H, P → H, and M → P transitions, based upon mean-field theories. The M → H and P → H transitions were determined with the RPA, and the M → P transition was determined with SCFT (based upon the ability to converge upon a d-spacing). The theoretical calculations extend only up to 134 °C (above this temperature, no theoretical predictions could be made due to our inability to measure χ_{BC}). The dashed curve connects experimental data points above 134 °C.

It is remarkable that this blend, which did not show any evidence of a homogeneous phase at atmospheric pressure, has a significant homogeneous window once pressure is elevated. Our studies show that the reason for the homogenization is twofold. First, χ_{AB} decreases as the pressure is increased and even becomes negative at the highest pressures and temperatures. Figure 4 shows the values for $\chi_{AB}N_{AVE}$, which is greater than 2 when A and B are immiscible as a function of T and P. It is clear when looking at Figure 4 that the effect of decreasing χ_{AB} alone is not enough to explain the homogeneous phase window in Figure 8. For example, at 70 °C and 0.62 kbar, the RPA predicted a homogeneous phase with no fitting parameters. However, $\chi_{AB}N_{AVE} = 2.80$, which is well above 2. The homogenization at 70 °C and 0.62 kbar is due to the presence of the A−C surfactant. The second reason for the observed pressure dependence of the A/B/A−C blend is that χ_{BC} becomes more negative as the pressure is increased. It is thus clear that the combination of the pressure effects on χ_{AB} and χ_{BC} are responsible for the formation of the homogeneous phase at high pressures.

Conclusion

We have probed the effect of pressure on the thermodynamic properties of a ternary mixture of two homopolymers A and B and an A−C diblock copolymer. At atmospheric pressure, this blend formed a lamellar phase at low temperatures, a microemulsion at intermediate temperatures, and macrophase separation at high temperatures.[29] Upon pressurization, a homogeneous phase was observed across a wide range of pressures and temperatures. This is qualitatively different from the phase behavior of oil/water/nonionic surfactant mixtures[47−62] wherein the phase separated window is seen to broaden with increasing pressure. In an attempt to understand the underpinnings of this phase behavior, the effect of pressure on the binary interaction parameters was measured. We found that χ_{AB} and χ_{BC} decreased with increasing pressure, while χ_{AC} was insensitive to changes in pressure. SCFT, RPA, and FHT, with binary parameters as inputs, were used to predict the thermodynamic properties of our A/B/A−C blend. This enabled distinguishing between microphase separated states, homogeneous states with and

without periodic concentration fluctuations, and macrophase separation. SCFT calculations of the domain size of the microphase separated states as a function of pressure and temperature were within 10% of the experimental value across the entire accessible range. Previous work showed that FHT can be used to describe the phase behavior of binary homopolymer blends at elevated pressures as long as the pressure and temperature dependencies of χ_{mn}, l_m, and v_m are determined.[14,25,26] The present study extends this idea to show that mean-field theories (RPA, SCFT, FHT) can be used to describe the pressure dependent thermodynamics of complex multicomponent systems that are characterized by periodic concentration fluctuations as well as microphase and macrophase separated states.

Acknowledgment. This material is based upon work supported by the National Science Foundation under Grants 0305711 and 0504122**.** We acknowledge the support of the National Institute of Standards and Technology, U.S. Department of Commerce, in providing the neutron research facilities used in this work.

References and Notes

(1) Flory, P. J. *J. Chem. Phys.* **1942**, *10*, 51−61.
(2) Huggins, M. L. *J. Phys. Chem.* **1942**, *46*, 151−158.
(3) Balsara, N. P.; Fetters, L. J.; Hadjichristidis, N.; Lohse, D. J.; Han, C. C.; Graessley, W. W.; Krishnamoorti, R. *Macromolecules* **1992**, *25*, 6137−6147.
(4) Balsara, N. P. In *Physical Properties of Polymers Handbook*; Mark, J. E., Ed.; AIP Press: New York, 1996; pp 257−268.
(5) Kwei, T. K.; Nishi, T.; Roberts, R. F. *Macromolecules* **1974**, *7*, 667−674.
(6) Rappl, T. J.; Balsara, N. P. *J. Chem. Phys.* **2005**, *122*.
(7) Ryu, D. Y.; Lee, D. H.; Jang, J.; Kim, J. K.; Lavery, K. A.; Russell, T. P. *Macromolecules* **2004**, *37*, 5851−5855.
(8) Balsara, N. P.; Rappl, T. J.; Lefebvre, A. A. *J. Polym. Sci., Part B: Polym. Phys.* **2004**, *42*, 1793−1809.
(9) Lipson, J. E. G.; Tambasco, M.; Willets, K. A.; Higgins, J. S. *Macromolecules* **2003**, *36*, 2977−2984.
(10) Lefebvre, A. A.; Lee, J. H.; Balsara, N. P.; Vaidyanathan, C. *J. Chem. Phys.* **2002**, *117*, 9063−9073.
(11) Lefebvre, A. A.; Lee, J. H.; Balsara, N. P.; Vaidyanathan, C. *J. Chem. Phys.* **2002**, *117*, 9074−9083.
(12) Lefebvre, A. A.; Balsara, N. P.; Lee, J. H.; Vaidyanathan, C. *Macromolecules* **2002**, *35*, 7758−7764.
(13) Lefebvre, A. A.; Lee, J. H.; Balsara, N. P.; Hammouda, B. *J. Chem. Phys.* **2002**, *116*, 4777−4781.
(14) Lefebvre, A. A.; Lee, J. H.; Balsara, N. P.; Hammouda, B. *Macromolecules* **2000**, *33*, 7977−7989.
(15) Lefebvre, A. A.; Lee, J. H.; Balsara, N. P.; Hammouda, B. *J. Polym. Sci., Part B: Polym. Phys.* **2000**, *38*, 1926−1930.
(16) Lefebvre, A. A.; Lee, J. H.; Jeon, H. S.; Balsara, N. P.; Hammouda, B. *J. Chem. Phys.* **1999**, *111*, 6082−6099.
(17) Balsara, N. P.; Lefebvre, A. A.; Lee, J. H.; Lin, C. C.; Hammouda, B. *AIChE J.* **1998**, *44*, 2515−2519.
(18) Rabeony, M.; Lohse, D. J.; Garner, R. T.; Han, S. J.; Graessley, W. W.; Migler, K. B. *Macromolecules* **1998**, *31*, 6511−6514.
(19) Beiner, M.; Fytas, G.; Meier, G.; Kumar, S. K. *Phys. Rev. Lett.* **1998**, *81*, 594−597.
(20) Hammouda, B.; Balsara, N. P.; Lefebvre, A. A. *Macromolecules* **1997**, *30*, 5572−5574.
(21) Hammouda, B.; Benmouna, M. *J. Polym. Sci., Part B: Polym. Phys.* **1995**, *33*, 2359−2364.
(22) Hammouda, B.; Bauer, B. J. *Macromolecules* **1995**, *28*, 4505−4508.
(23) Janssen, S.; Schwahn, D.; Springer, T.; Mortensen, K. *Macromolecules* **1995**, *28*, 2555−2560.
(24) Janssen, S.; Schwahn, D.; Mortensen, K.; Springer, T. *Macromolecules* **1993**, *26*, 5587−5591.
(25) Lefebvre, K. K.; Lee, J. H.; Balsara, N. P.; Hammouda, B.; Krishnamoorti, R.; Kumar, S. *Macromolecules* **1999**, *32*, 5460−5462.
(26) Prausnitz, J. M. *Molecular Thermodynamics of Fluid-Phase Equilibria*; Prentice Hall PTR: Upper Saddle River, NJ, 1999.
(27) Ruzette, A. V. G.; Mayes, A. M.; Pollard, M.; Russell, T. P.; Hammouda, B. *Macromolecules* **2003**, *36*, 3351−3356.
(28) Lee, J. H.; Ruegg, M. L.; Balsara, N. P.; Zhu, Y. Q.; Gido, S. P.; Krishnamoorti, R.; Kim, M. H. *Macromolecules* **2003**, *36*, 6537−6548.
(29) Reynolds, B. J.; Ruegg, M. L.; Balsara, N. P.; Radke, C. J.; Shaffer, T. D.; Lin, M. Y.; Shull, K. R.; Lohse, D. J. *Macromolecules* **2004**, *37*, 7401−7417.
(30) Xu, Z.; Jandt, K. D.; Kramer, E. J.; Edgecombe, B. D.; Frechet, J. M. J. *J. Polym. Sci., Part B: Polym. Phys.* **1995**, *33*, 2351−2357.
(31) Shull, K. R.; Kellock, A. J.; Deline, V. R.; Macdonald, S. A. *J. Chem. Phys.* **1992**, *97*, 2095−2104.
(32) Adedeji, A.; Hudson, S. D.; Jamieson, A. M. *Macromolecules* **1996**, *29*, 2449−2456.
(33) Adedeji, A.; Lyu, S.; Macosko, C. W. *Macromolecules* **2001**, *34*, 8663−8668.
(34) Ruegg, M. L.; Reynolds, B. J.; Lin, M. Y.; Lohse, D. J.; Balsara, N. P. *Macromolecules* **2006**, *39*, 1125−1134.
(35) Lee, J. H. Ph.D. Thesis, Chemical Engineering, University of California, Berkeley, 2002.
(36) Kahlweit, M.; Strey, R. *Angew. Chem., Int. Ed. Engl.* **1985**, *24*, 654−668.
(37) Kahlweit, M.; Strey, R.; Firman, P.; Haase, D. *Langmuir* **1985**, *1*, 281−288.
(38) Kahlweit, M.; Strey, R.; Haase, D.; Firman, P. *Langmuir* **1988**, *4*, 785−790.
(39) Strey, R. *Colloid Polym. Sci.* **1994**, *272*, 1005−1019.
(40) Chen, S. H.; Choi, S. *Supramol. Sci.* **1998**, *5*, 197−206.
(41) Magid, L.; Butler, P.; Payne, K.; Strey, R. *J. Appl. Crystallogr.* **1988**, *21*, 832−834.
(42) Bates, F. S.; Maurer, W.; Lodge, T. P.; Schulz, M. F.; Matsen, M. W.; Almdal, K.; Mortensen, K. *Phys. Rev. Lett.* **1995**, *75*, 4429−4432.
(43) Hillmyer, M. A.; Maurer, W. W.; Lodge, T. P.; Bates, F. S.; Almdal, K. *J. Phys. Chem. B* **1999**, *103*, 4814−4824.
(44) Bates, F. S.; Maurer, W. W.; Lipic, P. M.; Hillmyer, M. A.; Almdal, K.; Mortensen, K.; Fredrickson, G. H.; Lodge, T. P. *Phys. Rev. Lett.* **1997**, *79*, 849−852.
(45) Washburn, N. R.; Lodge, T. P.; Bates, F. S. *J. Phys. Chem. B* **2000**, *104*, 6987−6997.
(46) Morkved, T. L.; Chapman, B. R.; Bates, F. S.; Lodge, T. P.; Stepanek, P.; Almdal, K. *Faraday Discuss.* **1999**, 335−350.
(47) Kahlweit, M.; Strey, R.; Firman, P.; Haase, D.; Jen, J.; Schomacker, R. *Langmuir* **1988**, *4*, 499−511.
(48) Sassen, C. L.; Filemon, L. M.; Deloos, T. W.; Arons, J. D. *J. Phys. Chem.* **1989**, *93*, 6511−6516.
(49) Sassen, C. L.; Casielles, A. G.; Deloos, T. W.; Arons, J. D. *Fluid Phase Equilib.* **1992**, *72*, 173−187.
(50) Ferdinand, S.; Lesemann, M.; Paulaitis, M. E. *Langmuir* **2000**, *16*, 10106−10114.
(51) Sassen, C. L.; Deloos, T. W.; Arons, J. D. *J. Phys. Chem.* **1991**, *95*, 10760−10763.
(52) Andersen, J. G.; Koak, N.; de Loos, T. W. *Fluid Phase Equilib.* **1999**, *163*, 259−273.
(53) McFann, G. J.; Johnston, K. P. *Langmuir* **1993**, *9*, 2942−2948.
(54) Nagao, M.; Seto, H.; Ihara, D.; Shibayama, M.; Takeda, T. *J. Chem. Phys.* **2005**, *123*.
(55) Eastoe, J.; Steytler, D. C.; Robinson, B. H.; Heenan, R. K. *J. Chem. Soc., Faraday Trans.* **1994**, *90*, 3121−3127.
(56) Seto, H.; Nagao, M.; Kawabata, Y.; Takeda, T. *J. Chem. Phys.* **2001**, *115*, 9496−9502.
(57) Nagao, M.; Seto, H.; Takeda, T.; Kawabata, Y. *J. Chem. Phys.* **2001**, *115*, 10036−10044.
(58) Nagao, M.; Seto, H. *Phys. Rev. E* **1999**, *59*, 3169−3176.
(59) Nagao, M.; Seto, H.; Okuhara, D.; Okabayashi, H.; Takeda, T.; Hikosaka, M. *Physica B* **1997**, *241*, 970−972.
(60) Saidi, Z.; Daridon, J. L.; Boned, C. *J. Phys. D: Appl. Phys.* **1995**, *28*, 2108−2112.
(61) Beckman, E. J.; Smith, R. D. *J. Phys. Chem.* **1991**, *95*, 3253−3257.
(62) Kaler, E. W.; Billman, J. F.; Fulton, J. L.; Smith, R. D. *J. Phys. Chem.* **1991**, *95*, 458−462.
(63) Krishnamoorti, R. Unpublished data.
(64) Glinka, C. J.; Barker, J. G.; Hammouda, B.; Krueger, S.; Moyer, J. J.; Orts, W. J. *J. Appl. Crystallogr.* **1998**, *31*, 430−445.
(65) Kline, S. NIST Center for Neutron Research, 2001.
(66) Balsara, N. P.; Lohse, D. J.; Graessley, W. W.; Krishnamoorti, R. *J. Chem. Phys.* **1994**, *100*, 3905−3910.
(67) Flory, P. J. *J. Chem. Phys.* **1941**, *9*, 660.
(68) Huggins, M. *J. Chem. Phys.* **1941**, *9*, 440.
(69) Benoit, H.; Benmouna, M.; Wu, W. L. *Macromolecules* **1990**, *23*, 1511−1517.
(70) Akcasu, A. Z.; Tombakoglu, M. *Macromolecules* **1990**, *23*, 607−612.
(71) de Gennes, P. G. *Scaling Concepts in Polymer Physics*; Cornell University Press: Ithaca, NY, 1979.

(72) Thompson, R. B.; Matsen, M. W. *J. Chem. Phys.* **2000**, *112*, 6863−6872.
(73) Werner, A.; Schmid, F.; Binder, K.; Muller, M. *Macromolecules* **1996**, *29*, 8241−8248.
(74) Shull, K. R.; Mayes, A. M.; Russell, T. P. *Macromolecules* **1993**, *26*, 3929−3936.
(75) Janert, P. K.; Schick, M. *Macromolecules* **1997**, *30*, 137−144.
(76) Lohse, D. J.; Garner, R. T.; Graessley, W. W.; Krishnamoorti, R. *Rubber Chem. Technol.* **1999**, *72*, 569−579.
(77) Krishnamoorti, R. *Rubber Chem. Technol.* **1999**, *72*, 580−586.
(78) Krishnamoorti, R.; Graessley, W. W.; Fetters, L. J.; Garner, R. T.; Lohse, D. J. *Macromolecules* **1995**, *28*, 1252−1259.
(79) Graessley, W. W.; Krishnamoorti, R.; Balsara, N. P.; Butera, R. J.; Fetters, L. J.; Lohse, D. J.; Schulz, D. N.; Sissano, J. A. *Macromolecules* **1994**, *27*, 3896−3901.
(80) In this paper, all calculations were conducted using the pressure dependencies of χ (with the *D*, *E*, and *F* coefficients). The temperature dependencies of χ were used to interpolate between the temperatures at which the interaction parameters were measured. The interpolated values of χ were then refit to find the *D*, *E*, and *F* coefficients at each temperature. The following are the *D*, *E*, and *F* coefficients obtained from the interpolation (all pressures are in kbar). For A/B interactions: $T = 50$ °C: $D = 4.52 \times 10^{-3}$, $E = -1.86 \times 10^{-3}$, $F = -2.09 \times 10^{-7}$. $T = 90$ °C: $D = 4.91 \times 10^{-3}$, $E = -1.29 \times 10^{-3}$, $F = -2.12 \times 10^{-5}$. $T = 130$ °C: $D = 5.05 \times 10^{-3}$, $E = -1.14 \times 10^{-3}$, $F = 7.29 \times 10^{-5}$. For B/C interactions: $T = 50$ °C: $D = -3.13 \times 10^{-3}$, $E = -2.24 \times 10^{-3}$, $F = -1.36 \times 10^{-5}$. $T = 90$ °C: $D = -5.76 \times 10^{-4}$, $E = -1.83 \times 10^{-3}$, $F = 2.36 \times 10^{-5}$. $T = 110$ °C: $D = 2.90 \times 10^{-4}$, $E = -1.95 \times 10^{-3}$, $F = 1.11 \times 10^{-4}$. $T = 130$ °C: $D = 9.64 \times 10^{-4}$, $E = -2.19 \times 10^{-3}$, $F = 2.26 \times 10^{-4}$. A/C interactions were assumed to be pressure-independent. Because of experimental uncertainties, slightly different results are obtained if pressure-dependent values of *A*, *B*, and *C* coefficients are used. The differences are within the uncertainties of the χ measurements.
(81) Maurer, W. W.; Bates, F. S.; Lodge, T. P.; Almdal, K.; Mortensen, K.; Fredrickson, G. H. *J. Chem. Phys.* **1998**, *108*, 2989−3000.
(82) Teubner, M.; Strey, R. *J. Chem. Phys.* **1987**, *87*, 3195−3200.
(83) Morkved, T. L.; Stepanek, P.; Krishnan, K.; Bates, F. S.; Lodge, T. P. *J. Chem. Phys.* **2001**, *114*, 7247−7259.
(84) Gompper, G.; Holyst, R.; Schick, M. *Phys. Rev. A* **1991**, *43*, 3157−3160.

MA061894W